Internal Structure of the Precordilleran Fault System (Chile): Insights from Structural and Geophysical Observations

C. Janssen (1), A. Hoffmann-Rothe (1) , H. Brasse (2)

(1) GeoForschungsZentrum Potsdam, Telegrafenberg D 425, D-14473 Potsdam,
(2) FU Berlin, Geophysik, Malteserstr. 74-100, D-1249 Berlin
e-mail: jans@gfz-potsdam.de

GEOFORSCHUNGSZENTRUM POTSDAM
STIFTUNG DES ÖFFENTLICHEN RECHTS

Introduction

In zones of oblique convergence, like between the Pacific Nazca-plate and South America, the strike slip component of relative movement is taken up by major continental faults. The kinematics and mechanics of faulting may yield information on the rheological structure of the overriding plate (Molnar, 1992). The Andes display some excellent examples of strike-slip fault zones in the fore-arc region, e.g. the Precordilleran Fault system (**Fig.1**), that allow to address important questions concerning the geometry, kinematics and strength of these fault zones. In particular, some uncertainties still exist regarding the variations of fault zone characteristics (thickness and depth of fault core and damaged zone, deformation mechanisms, fluid flow) both along and across the fault system.

Here, we examine the Fracture Process Zone (FPZ) of the West Fissure Shear System by a combination of structural and electromagnetic studies.

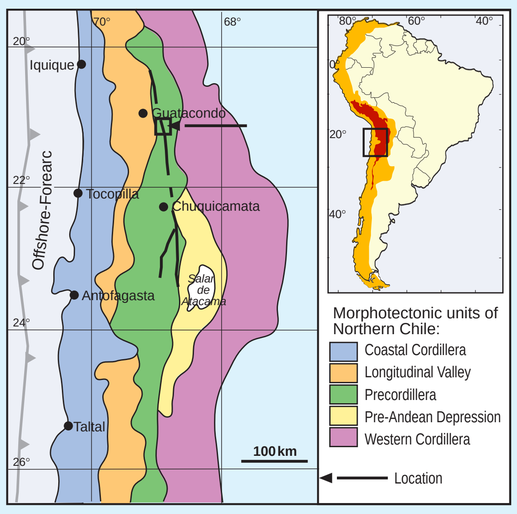

Fig.1 *: Overview sketch of Northern Chile and profile location indicated by arrow (slightly modified after Pelz et al., 1998).*

Geological Setting

The West Fissure Zone (WFZ) as part of the Precordilleran Fault system is well exposed for about 170 km from Calama northward to Quebrada Blanca (Dilles et al., 1997). The fault zone has been active since the Late Eocene/ Early Oligocene (Reuter et al., 1996). An older dextral strike-slip motion caused by subduction related magmatic arc tectonics (Incaic tectonic phase) is followed by sinistral shear corresponding to a period of reduced convergence rate and possibly reduced plate coupling (Reutter et al. 1996). During the youngest event dextral strike slip was reactivated. The tectonic inversion of the fault system is also reflected in varying amount of displacement (dextral displacement: 0.5 - 2 km, sinistral displacement: 35-37 km; Reutter et al., 1991; Tomlinson et al., 1997a,b).

Our investigation concentrates on several localities along a profile crossing the WFZ between 20°54' – 20°58' S (**Fig.2** and **Fig.3a**). Deformation structures including folds, foliations, brittle faults and thrusts, trend obliquely to the main fault trace (Carrasco et al., 1999).

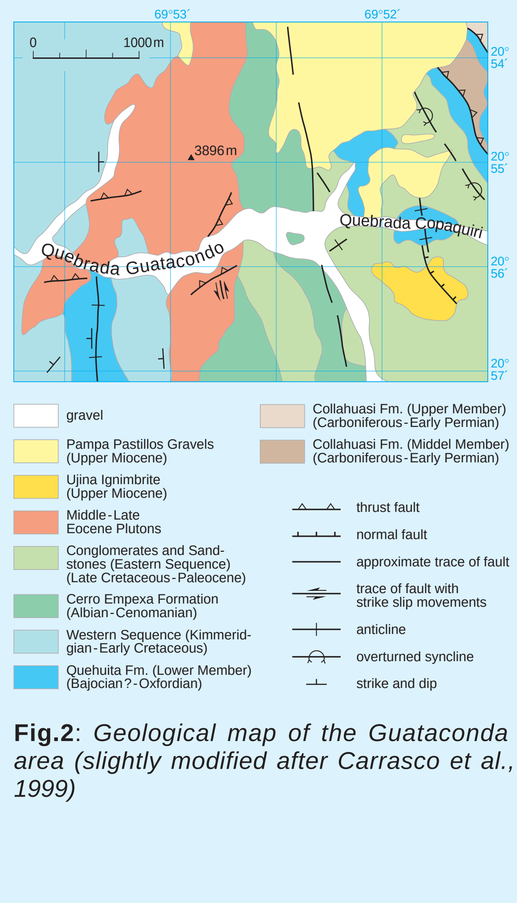

Fig.2: *Geological map of the Guataconda area (slightly modified after Carrasco et al., 1999)*

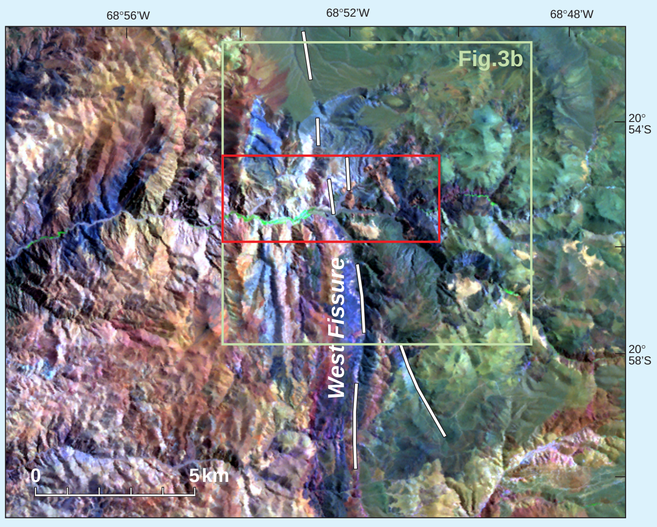

Fig.3a: *Satellite image of the Guataconda region with trace of the West Fissure. The red rectangular area marks the investigated.*

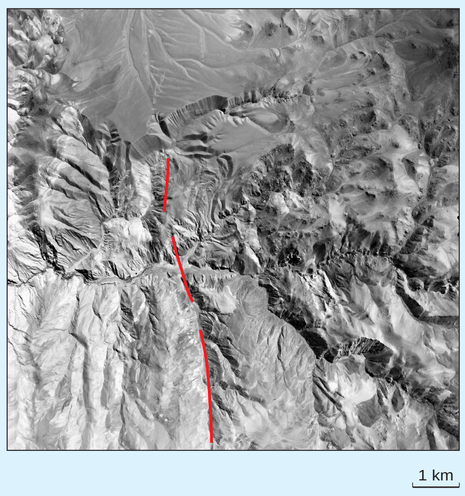

Fig.3b: *Aerial photograph of the investigated area.*

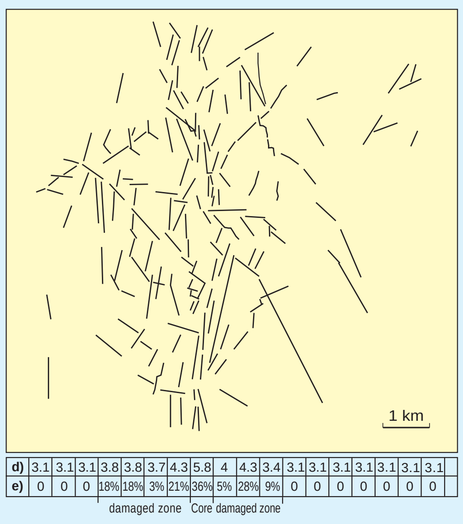

Fig.3c: *Distribution of fracture patterns derived from* **Fig.3b***;* (**d**) *average fracture density;* (**e**) *Degree of orientation (see text).*

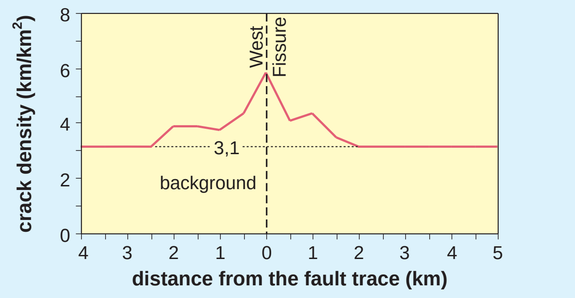

Fig. 4: *Fracture densities along the investigated profile*

Audio-Frequency Magnetotelluric

Only in the high frequency range from 500 Hz-1Hz a superficial conductivity anomaly reaching a depth of 100 m at maximum can be observed and modelled in the position of the fault (**Fig.6**). The width of this zone reaches approx. 110 m at the surface. A fault related lateral conductivity contrast is not obvious at greater depths (> 300 m).

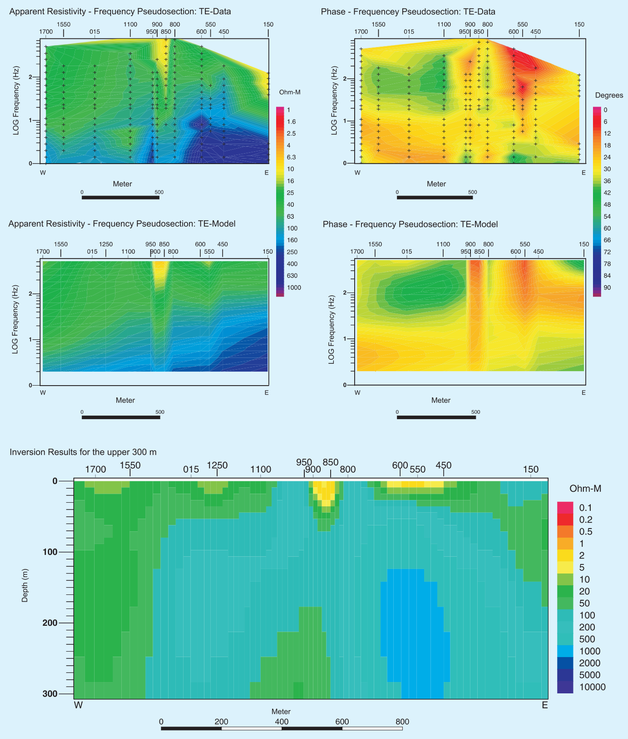

Fig.6: *Magnetotelluric data (upper two sections) and the electrical resistivity model (bottom). The sections in the middle show the model response.*

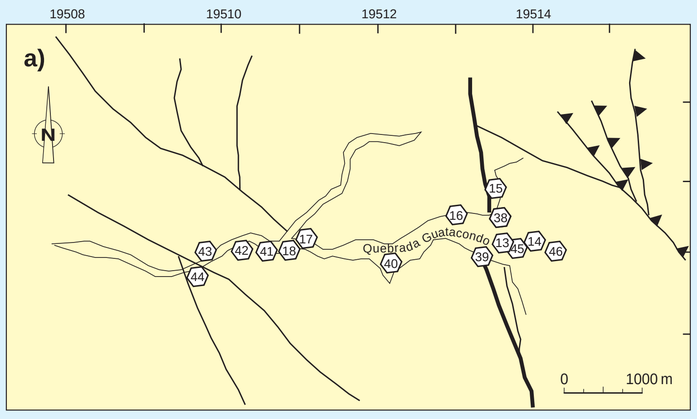

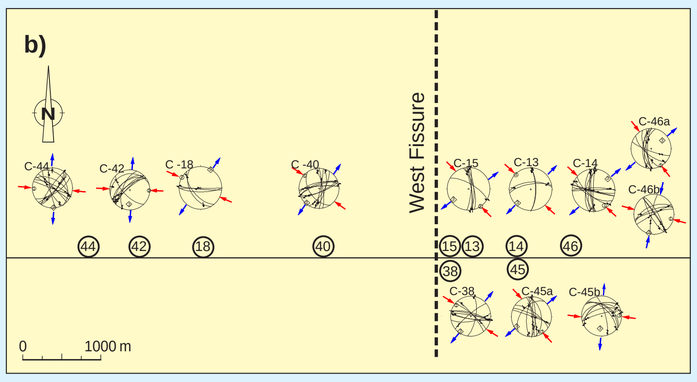

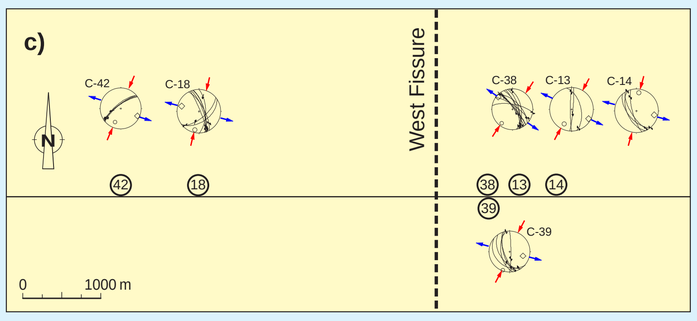

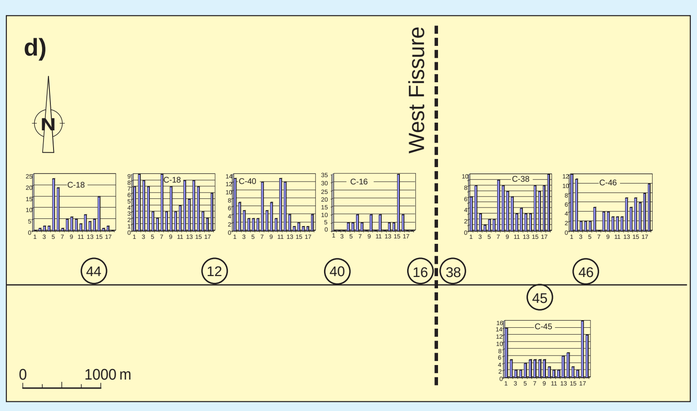

Fig. 5: (**a**) *Geotectonic map of the WFZ with the locations along the profile of detailed investigation;* (**b**) *Fault plane and fault slip data of the older deformation event (red and black arrows represent the shortening and extension axes, respectively);* (**c**) *Fault plane and fault slip data of the younger deformation event;* (**d**) *Fracture orientation (the numbers on the x-axis denote 0-180°).*

Satellite image and aerial photographs of the WFFZ

To analyse the larger scale structural patterns we used satellite images and aerial photgraphs (**Fig.3a** and **b**). **Fig. 3c** shows the distribution of fracture patterns derived from the aerial photograph of the Guataconda region.The WFZ does not form a continuous trace. Instead, at the surface the fault is characterized by a number of distinct but inter-related fracture lines. We observe a rapid decrease in the average fracture density with increasing distance to the fault plane (fracture densities were measured as the total length of fractures in km per unit area (Underwood, 1970; **Fig.3d**). This density decrease is symmetrically on both sides of the fault (**Fig.4**). The analysis of the fracture lines in terms of strike reveals a fairly complicated fracture network with two main sets, namely NNW-SSE and NNE-SSW striking fractures (**Fig.3c** and **e**; the percentages for the degree of orientation refer to the number of traces orientated subparallel to the fault). The major fracture directions are more or less parallel or form a low angle to the direction of the WFZ. According to our field work we assume that these fracture sets are mainly secondary faults related to the WFZ.

Kinematic analysis

Kinematic analysis of fault slip data have revealed two faulting events with constant orientation of principal strain axes that dominate the fault patterns within the Guataconda area. (first event: NW-SE shortening and NE-SW extension, **Fig.5a**; second event: reverse orientation, **Fig.5b**). These orientations can be observed on both sides of the fault. Further away from the main fault trace (100 m, 300 m, 800 m, up to 2000 m) the composite strain axes indicate once again the same directions. The uniform orientation of principal strain axes suggests that the whole FPZ is kinematically coherent.

At distances of about 2500 to 3000 m from the main fault trace the direction of principal strain axes changes (E-W shortening and N-S extension; **Fig.5b**).

The fracture orientations measured in the selected outcrops vary among the different study areas as illustrated by the histograms in **Fig. 5d**. More than one maximum of fracture orientation can be found for all locations. The fractures are mostly oriented in the range 0-40° (50°), 70-100° and 160-180°. In contrast to the results from the aerial photograph analysis the fracture orientation on the outcrop scale is not affeceted by the fault.

Conclusions

Geological field work and magnetotelluric data from one profile across the WFZ in northern Chile were used to describe the geometry and structure of the fracture process zone surrounding the strike-slip fault. The width of the FPZ based on the fracture density distribution is 4000 m (**Fig.7a**). The fracture density reaches a maximum in the fault core. The width of the process zone corresponds to the region where the fault is kinematically uniform (**Fig.7b**).

The Audio-Frequency Magnetotelluric (AMT) imaging shows a low electrical resistivity zone (apparent resistivity of 2-20 Ωm) congruent with the mapped surface trace of the fault. This conductivity enhancement is probably due to meteoric water entering a zone of ruptured rocks along the fault trace. However, in contrast to the broad process zone, this zone is very narrow (100 m) and only 100 m deep (**Fig.7c**). We assume that the discrepancy may be related to cyclical fault evolution. At present, we have no indication for seismic slip along the investigated segment of the West Fissure. Fault models have shown that during aseismic periods of fault evolution fault healing (i.e. strength recovery) due to compaction and cementation is active. Hence, fluids and fluid transport, which are probably responsible for enhanced conductivity, are confined to the fault core.

References

Carrasco P.; Wilke H. and Scheider H. (1999): Post Eocene deformational events in the North segment of the precordilleran Fault system, Copaquiri (21°S). Fourth ISAG, Goettingen (germany), 04-06/10/99

Dilles, J.H.T., A.J.; Martin, M.W. and Blanco, N., (1997): El Abra and Fortuna Complexes: A porphyry copper batholit sinistrally displaced by the Falla Oeste: Actas, v. III.

Molnar, P. 1992): Brace-goetze Strength Profiles, the Partitioning of Strike-slip and thrust Faulting at Zones of Oblique Convergence, and the Stress-Heat Flow Paradox of the San Andreas Fault, In: Fault mechanics and transport properties of rocks, ed. B. Evans, B. and Wong, T.F., Academic press

Reutter K.J.; Scheuber E. and Helmcke, D., (1991): structural evidence of orogen-parallel strike slip displacements in the Precordillera of northern Chile: Geol Rundschau, v. 80, p. 135-153.

Reutter K.J.; Scheuber E. and Chong, G., (1996): The Precordilleran fault system of Chuquicamata, Northern Chile: evidence for reversals along arc-parallel strike-slip faults: Tectonophysics, v. 259, p. 213-228.

Tomlinson, A.J.a.B., N., (1997): Structural evolution and displacement history of the west fault system, Precordillera, Chile: Part 1, synmineral history: Actas, v. III.

Tomlinson, a.a.B., N., (1997): Structural evolution and displacement history of the west fault system, Precordillera, Chile: Part 1, synmineral history: Actas, v. III.

Underwood, E.E., (1970): Quantitative Stereology: Wesly Publishing Company, 274 p.

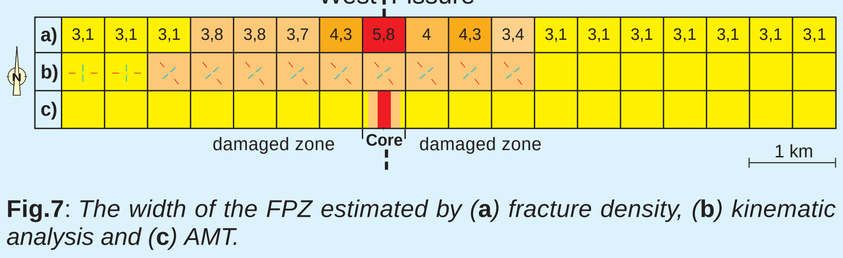

Fig.7: *The width of the FPZ estimated by* (**a**) *fracture density,* (**b**) *kinematic analysis and* (**c**) *AMT.*